Available online at www.sciencedirect.com
SCIENCE DIRECT®
Chemistry and Physics of Lipids 126 (2003) 211–223
CPL
CHEMISTRY AND PHYSICS OF LIPIDS
www.elsevier.com/locate/chemphyslip

Interpretation of small angle X-ray measurements guided by molecular dynamics simulations of lipid bilayers

Jonathan N. Sachs [a], Horia I. Petrache [b,*], Thomas B. Woolf [c]

[a] *Department of Biomedical Engineering, The Johns Hopkins University School of Medicine, Baltimore, MD 21205, USA*
[b] *Laboratory of Physical and Structural Biology, NICHD, National Institutes of Health, Bldg. 9, Rm 1E116, Bethesda, MD 20892, USA*
[c] *Department of Physiology, The Johns Hopkins University School of Medicine, Baltimore, MD 21205, USA*

Received 25 June 2003; received in revised form 13 August 2003; accepted 13 August 2003

Abstract

Reconstruction and interpretation of lipid bilayer structure from X-ray scattering often rely on assumptions regarding the molecular distributions across the bilayer. It is usually assumed that changes in head–head spacings across the bilayer, as measured from electron density profiles, equal the variations in hydrocarbon thicknesses. One can then determine the structure of a bilayer by comparison to the known structure of a lipid with the same headgroup. Here we examine this procedure using simulated electron density profiles for the benchmark lipids DMPC and DPPC. We compare simulation and experiment in both real and Fourier space to address two main aspects: (i) the measurement of head–head spacings from relative electron density profiles, and (ii) the determination of the absolute scale for these profiles. We find supporting evidence for the experimental procedure, thus explaining the robustness and consistency of experimental structural results derived from electron density profiles. However, we also expose potential pitfalls in the Fourier reconstruction that are due to the limited number of scattering peaks. Volumetric analysis of simulated bilayers allows us to propose an improved, yet simple method for scale determination. In this way we are able to remove some of the restrictions imposed by limited scattering data in constructing reliable electron density profiles.

Keywords: Bilayer thickness; Electron density profile; Lipid headgroup; Fourier reconstruction; Form factors; Lipid volume

1. Introduction

X-ray diffraction studies of lipid bilayers have been specifically geared towards elucidation of the electron density profile, from which structural parameters such as the bilayer thickness, D_B, and the area per lipid, A, can be calculated (Nagle and Tristram-Nagle, 2000). Obtaining accurate estimates of these quantities is important for two main reasons. First, the close matching between the bilayer thickness and the hydrophobic part of membrane proteins appear to control protein function (Huang, 1986; Bloom et al., 1991; Harroun et al., 1999). It has been hypothesized that structural matching is biologically regulated via selection of lipids with proper chain length and saturation (Bloom et al., 1999). Depending on the length and saturation, bilayer thicknesses can differ by 10–15 Å (Rand and Parsegian, 1989; Nagle and Tristram-Nagle, 2000).

Abbreviations: DMPC, dimyristoylphosphatidylcholine; DPPC, dipalmitoylphosphatidylcholine

* Corresponding author. Tel.: +1-301-402-4698; fax: +1-301-402-9462.
E-mail address: horia@helix.nih.gov (H.I. Petrache).

0009-3084/$ – see front matter © 2003 Elsevier Ireland Ltd. All rights reserved.
doi:10.1016/j.chemphyslip.2003.08.001

Yet, significantly more subtle variations are known to influence ion channel lifetimes (Elliott et al., 1983) and conformations (Greathouse et al., 1994), as well as the orientations of hydrophobic helical peptides (Killian and Heijne, 2000; Petrache et al., 2000, 2002). Similarly, structural properties associated with the lipid cross-sectional area and lateral stress (Gruner, 1989; Brown, 1994; Botelho et al., 2002) are known to modulate protein function, as well as membrane permeability.

Second, accurate measurements of structural parameters are needed for quantification of interbilayer interactions (McIntosh and Simon, 1986a; Rand and Parsegian, 1989; Israelachvili, 1992; Leikin et al., 1993; Zimmerberg and Chernomordik, 1999). At small distances, interbilayer forces depend exponentially on the interbilayer separation, changing by 20% with a 1 Å change in separation (McIntosh and Simon, 1986a, 1993; Marsh, 1989; Rand and Parsegian, 1989; Petrache et al., 1998a). Here the relevant structural parameter is the water spacing D_W, which is calculated from the lamellar repeat D, as $D_W = D - D_B$. The accuracy of D_W then depends on the determination of D_B.

Measuring structural parameters for soft, highly fluctuating materials such as the lipid membrane, is a difficult task. Structural descriptions are more readily obtained for the lower temperature states: gel (Nagle and Wiener, 1989; Sun et al., 1996a; Tristram-Nagle et al., 2002), subgel (Tristram-Nagle et al., 1994; Katsaras, 1995) and, obviously, crystal (Small, 1986), where lipid hydrocarbon chains are ordered. Both normal (thickness) and lateral (cross-sectional area) parameters can be determined directly from the low and the wide angle X-ray scattering, respectively. For the fluid (melted chain) phase, the apparent structural resolution is 5–10 Å, corresponding to the spatial extent of the molecular distributions, as presented by the electron density profiles (Worthington, 1969; Blaurock et al., 1971; Wiener and White, 1992). However, by parsing the lipid bilayer into molecular components, such as the lipid headgroup and acyl chains, *average* structural parameters are commonly reported with a precision of 1 Å or less (Rand and Parsegian, 1989; Nagle and Tristram-Nagle, 2000; Rawicz et al., 2000).

The most readily available parameter from the electron density profile is the spacing D_{HH} between the electron rich headgroup peaks. By itself, D_{HH} is not sufficient for a complete description of structure, because its relationship with lateral parameters (area per lipid, A) is complicated by the broad lipid–water interface. One needs to relate D_{HH} to better defined, and thermodynamically relevant parameters such as the hydrocarbon thickness D_C and the total bilayer thickness D_B, which are related to A through molecular volumes. Therefore, it is necessary to combine electron density and volumetric analyses in order to describe fluid phase bilayer structure (McIntosh and Simon, 1986b; Nagle et al., 1996; Petrache et al., 1997; Armen et al., 1998; Tristram-Nagle et al., 1998; Nagle and Tristram-Nagle, 2000).

Given the experimental scattering data, i.e. the form factor ratios $r_h = F_h/F_1$, there are two main methods to construct the electron density profile, $\rho^*(z)$. The first method is model-free and consists of direct Fourier reconstruction (Worthington, 1969),

$$\rho^*(z) - \rho^*_W = \frac{1}{D}F(0) + \frac{2}{D}F_1 \sum_{h=1}^{h_{max}} \alpha_h r_h \cos\left(\frac{2\pi h z}{D}\right), \quad (1)$$

where ρ^*_W is the bulk water electron density, D is the lamellar repeat spacing, $\alpha_h = \pm 1$ are form factor phases, and h_{max} is the number of observed diffraction orders. There are two quantities in Eq. (1) that are usually not available from X-ray. These are F_1, which in this formalism sets $\rho^*(z)$ on an absolute scale, and $F(0)$ which gives the total bilayer contrast (offset) relative to the water electron density ρ^*_W,

$$AF(0) = 2(n^*_L - \rho^*_W V_L) = 2(\rho^*_L - \rho^*_W)V_L, \quad (2)$$

in which A, V_L, and n^*_L denote the area, volume, and number of electrons per lipid molecule, respectively. Handling the scale has been an issue for the fluid phase, as this requires additional information or certain assumptions with regard to the shape of the electron density profile (Petrache et al., 1998b). The shape, however, is strongly influenced by the number of diffraction orders available, h_{max}, which truncate the sum in Eq. (1). Fourier truncates complicates comparison between lipid bilayers.

The second method for constructing electron density profiles is functional modeling. This is done by assuming a particular functional form for the bilayer profile, with a number of free parameters to be

determined by fitting to scattering form factors. Several approaches have been undertaken, from simple step-function models (Worthington, 1969), to more realistic Gaussian models (Nagle and Wiener, 1989; Wiener et al., 1989; Wiener and White, 1992) and to more detailed component models (Wiener and White, 1992; Schalke and Losche, 2000). Each of these models attempt to breakdown the electron density into component distributions by integrating knowledge from other measurements, such as specific volume, to reduce the number of fitting parameters.

Atomic-level computer simulations provide a new perspective on bilayer structure. There are numerous valuable contributions to the field addressing the underlying molecular disorder and heterogeneity (Chiu et al., 1995; Berger et al., 1997; Tieleman et al., 1997; Feller et al., 1997; Tobias et al., 1997; Smondyrev and Berkowitz, 1999; Huber et al., 2002). In the hierarchy of models just discussed, these in fact constitute the most elaborate. One consequence of such detail, however, is that molecular dynamics simulations cannot be cast as fitting procedures as with the models above, as tuning the force-field parameters to a particular scattering dataset is unfeasible. Of course, the aims of simulations are more ambitious than just modeling of electron density profiles, but in this work we will focus just on this aspect. Because simulated electron density profiles result from all-atom representations which implicitly obey volume conservation, they can be used to evaluate assumptions employed in structure determination from scattering data.

A "bootstrap" method has been used in the literature to obtain structural parameters for a new bilayer by comparison with a reference structure (McIntosh and Simon, 1986b; Nagle and Tristram-Nagle, 2000). It is assumed that the difference in the hydrocarbon thickness ΔD_C can be estimated from the shift of the headgroup peak, $\Delta D_{HH}/2$, if two lipids have the same headgroup. (A factor of 1/2 is needed because D_C is conventionally defined as half-thickness.) Having estimated D_C from the D_{HH} shift, the area per lipid is then obtained as the ratio between hydrocarbon volume and thickness. D_{HH} does not depend on $F(0)$ or the density scale, but needs to be corrected for Fourier truncation effects (Blaurock et al., 1971; Lesslauer et al., 1972). To minimize these effects, D_{HH} values have customarily been compared at similar resolution, D/h_{max} (McIntosh and Simon, 1986a,b, 1993; Rawicz et al., 2000), and correction terms were estimated using functional modeling (Sun et al., 1996a). With the availability of detailed atomic simulations, this aspect calls for renewed attention.

Here we consider previously reported MD simulations of fluid phase DMPC and DPPC bilayers as the basis for our discussion of structure determination from X-ray. We have focused on the Fourier reconstruction method and the calculation of the area per lipid from D_{HH} and density measurements. The main goal is a comprehensive exercise with electron density profiles, and not necessarily simulation refinement. We have used simulated bilayers with structural parameters within the experimental uncertainty (1.5% or better), as a scaffolding for construction of self-consistent methodologies for structure determination from experiment. Because the bilayer form factors are the primary X-ray data, we have compared simulation and experiment in the Fourier space. We show an overall agreement, especially in the low q range, which seems to have the major influence on the main structural parameters. We process the simulated continuous transform by artificial sampling and cutoff at high q-values to mimic the measurement of head–head spacing D_{HH}. We then compare D_{HH} differences between DMPC and DPPC with differences in the hydrocarbon thicknesses D_C to test the bootstrapping assumption. By analysis of Fourier truncation effects, we identify conditions for $\Delta D_C \approx \Delta D_{HH}/2$ and estimate a possible deviation range.

By comparison of continuous transforms, we identify and fix a scale discrepancy between simulation and experiment. We propose an improved method for setting experimental electron density profiles on an absolute scale by using structural and volumetric parameters obtainable from unscaled profiles. While not directly relevant for measurements of D_{HH} and subsequent determination of bilayer thicknesses, a correct absolute scale is critical for X-ray contrast (substitution) experiments (Franks et al., 1978).

2. Computational methods

2.1. Simulation setup

Simulations were performed using CHARMM software (Brooks et al., 1983) version 26 and were

previously reported (Petrache et al., 2002). Periodic boundary conditions were used with constant number of atoms (N), temperature (T), lateral area (A), and normal pressure (P_N) to generate NAP_NT ensembles. Two lipids were considered: dimyristoylphosphatidylcholine (DMPC), and dipalmitoylphosphatidylcholine (DPPC). Simulation temperatures were 30 °C for DMPC and 50 °C for DPPC. For both lipids, bilayers consisted of 36 lipid molecules. The normal pressure P_N was set to 1 atm, and the lateral area was set to $A = 59.7\,\text{Å}^2$ for DMPC (Petrache et al., 1998b) and $A = 62.9\,\text{Å}^2$ for DPPC (Nagle et al., 1996). The number of water molecules per lipid was 25.7 for DMPC and 29.1 for DPPC.

A full description of the simulation procedure is given elsewhere (Petrache et al., 2002). Briefly, lipid conformations were randomly chosen from a library of pre-equilibrated lipids in the fluid state. The DPPC library was provided by Hardy and Pastor (1994), and also used to generate DMPC molecules by deletion of two terminal carbon segments from each acyl chain. At least 12 bilayer configurations were generated for each lipid by reselecting from the libraries and by repeating equilibration steps that included elimination of steric conflicts. The resulting configurations were screened for characteristic properties of lipid bilayers in the fluid state (such as acyl chain and headgroup order), and the optimum structure was selected for each lipid. Such a rational approach to building a bilayer in the fluid state significantly minimizes the equilibration time. A cutoff of 12 Å was used for van der Waals interactions (Feller and Pastor, 1999), and particle mesh Ewald summation was used for electrostatic interactions. The time step was 2 fs, and all bonds involving hydrogens were fixed using the SHAKE algorithm, with a tolerance (relative deviation) of 10^{-6}. The frequency of regenerating the non-bonded list was set with a heuristic testing algorithm that updates based on the distance each atom moved since the last list update. Production dynamics simulations for each system were performed for 1.5 ns.

2.2. Volumetric calculations

Lipid volumes and decomposition into molecular components from simulation was done following Petrache et al. (1997) and Armen et al. (1998). A typical decomposition consists of four components: terminal methyl (CH_3), methylene (CH_2), lipid headgroup (includes carbonyls, glycerol and the phosphocholine group), and water. Corresponding number densities $n_3(z)$, $n_2(z)$, $n_H(z)$, and $n_W(z)$ as a function of location along the bilayer normal (z) are accumulated from the simulated trajectories and expressed in units of Å^{-3}. Component volumes, V_3, V_2, V_H, and V_W are then calculated as the values that make the total occupation probability,

$$p_T(z) = V_3 n_3(z) + V_2 n_2(z) + V_H n_H(z) + V_W n_W(z), \tag{3}$$

approach 1 for all values of z. Practically, the volumes are found by minimizing the function

$$\chi^2 = \sum_z [p_T(z) - 1]^2, \tag{4}$$

as detailed in Appendix A.

For calculation of bilayer thicknesses, following the Luzzati–Gibbs procedure, we divide the unit cell height, D, into a lipid thickness, D_B, and a water thickness, $D_W = D - D_B$ (Rand and Parsegian, 1989; Nagle and Tristram-Nagle, 2000). With cell volume conservation $AD = 2(V_L + n_W V_W)$, the bilayer thickness relates to D through the lipid volume fraction,

$$D_B = \frac{V_L}{V_L + n_W V_W} D. \tag{5}$$

We further divide the unit cell by decomposing D_B into a hydrocarbon thickness D_C and a headgroup thickness $D_H = D_B - D_C$. Volumetric thicknesses are related to the area per lipid through

$$A = \frac{2V_L}{D_B} = \frac{V_C}{D_C} = \frac{V_H}{D_H}, \tag{6}$$

where V_C and V_H are the hydrocarbon (both acyl chains) and the headgroup volume of one lipid.

From simulations, component volumes are calculated from p_T fits (Eq. (4)), then thicknesess are calculated from Eq. (6) using the area values.

2.3. Fourier transforms

Continuous Fourier transform $F(q)$ is calculated from the simulated $\rho^*(z)$ using

$$F(q) = \int_{-D/2}^{D/2} [\rho^*(z) - \rho_W^*] \cos(qz)\, dz, \tag{7}$$

where ρ_W^* is the electron density of water, and D is the average dimension of the simulation box. The experimental continuous transforms $F^{exp}(q)$, reproduced from Nagle et al. (1996) and Petrache et al. (1998b), have been calculated for samples with four orders of diffraction using the sampling theorem,

$$F^{exp}(q) = \sum_{h=-h_{max}}^{h_{max}} F_h \frac{\sin[(q-q_h)D/2]}{(q-q_h)D/2}, \quad (8)$$

where $h_{max} = 4$ and $q_h = 2\pi h/D$.

3. Results

3.1. Fourier truncation and head–head spacing D_{HH}

Simulated electron density profiles for DMPC at 30 °C and DPPC at 50 °C are shown in Fig. 1. Electrons were counted in bins of 0.1 Å (in the z-direction normal to the bilayer) and averaged over the simulation. The most prominent features of the profiles are the headgroup peaks at the lipid–water interface and the methyl troughs at the bilayer center. The two profiles shown are similar in shape, with DPPC being broader by about 2–3 Å due to its longer hydrocarbon chains. Relative to the water baseline, the headgroup region shows an excess of electrons and the hydrocarbon region an electron deficiency. It is this electronic contrast that makes the lipid bilayers visible to X-ray.

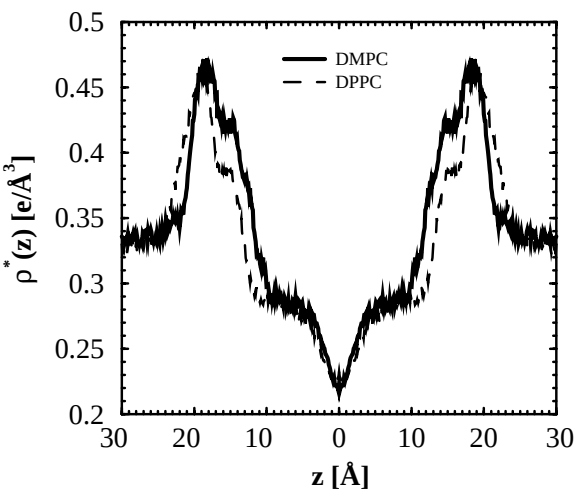

Fig. 1. Simulated electron density profiles, $\rho^*(z)$, for DMPC at 30 °C (solid line) and DPPC at 50 °C (dashed line). $\rho^*(z)$ is broader for DPPC due to its two additional methylene groups.

It is worth noting that while headgroup chemistry is the same for the two lipids, the headgroups peaks in Fig. 1 are different. This is due to differences in temperature, area per lipid, and water penetration in the headgroup region which influence spatial distributions (Feller et al., 1997; Mashl et al., 2001). The average distance across the bilayer between the phosphate atoms (D_{PP}) are 35.9 Å for DMPC and 39.0 Å for DPPC; they differ by 3.1 Å. To compare hydrocarbon regions we have calculated distances between C_2 carbons (belonging to the first methylene group next to the carbonyls). The average distances are 24.9 Å for DMPC and 27.7 Å for DPPC, a difference of 2.8 Å. The distance between phophorus and the C_2 carbon projected on the z-axis is 5.5 Å for DMPC and 5.7 Å for DPPC. These structural parameters, however, are not directly measurable in a typical X-ray experiment, rather, they are inferred from low-resolution electron density profiles.

In order to compare simulation with the raw X-ray data (form factors), we have calculated the continuous Fourier transforms, $F(q)$, of the simulated $\rho^*(z)$ using Eq. (7). In Fig. 2, we plot the absolute value $|F(q)|$ together with the experimental results from Petrache et al. (1998b) for DMPC and Nagle et al. (1996) for DPPC. Experimental form factors have been scaled such that all first order form factors lie on the simulated $F(q)$. The experimental continuous transforms $F^{exp}(q)$ have been calculated from samples with four orders of diffraction using the sampling theorem (Eq. (8)). There is a good overall agreement between the simulated $F(q)$ and the experimental form factor ratios. Still, noticeable differences exist. For DPPC, data in the first lobe ($h = 2$) are systematically slightly larger than the simulated $F(q)$; for DMPC there are deviations at the top of the first lobe. There is a good agreement for the third order, while for the fourth the simulated $F(q)$ is systematically smaller in magnitude than the experimental form factors. The values of $F(0)$, which give the average electronic contrast between lipid and water, agree very well between simulation and experiment for both lipids, suggesting that lipid and water densities are well reproduced. For DMPC, however, there is a noticeable discrepancy between the simulated and experimental scale of $F(q)$, which will be addressed in more detail below.

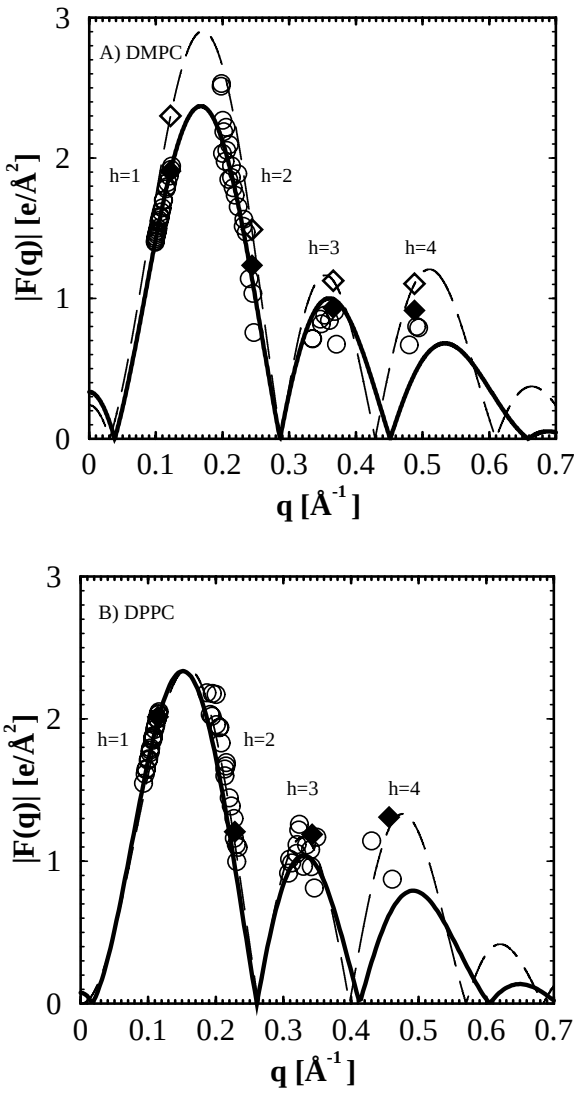

Fig. 2. Comparison between simulated continuous transforms, $F(q)$, (solid lines) and experimental form factors (symbols) taken from Petrache et al. (1998b) for DMPC (part A) and from Nagle et al. (1996) for DPPC (part B). First order form factors are set on the simulated $F(q)$. Experimentally derived continuous transforms, $F^{exp}(q)$, are shown with dashed lines. Solid diamonds indicate the samples used for reconstruction ($D = 51.5$ Å for DMPC and 55.1 Å for DPPC), scaled by the simulated $F(q)$. Open diamonds (DMPC only) show the same form factors scaled by $F^{exp}(q)$.

To compare structural parameters, we have calculated bilayer thicknesses within a Luzzati–Gibbs framework, as explained in Section 2. In this framework, thicknesses and cross-sectional areas are inversely related through the lipid volumes. The definitions we employ, as well as alternatives, have been recently reviewed by Nagle and Tristram-Nagle (2000). In the Luzzati–Gibbs framework, the bilayer thickness D_B, for example, corresponds to the z-plane where the probability of finding a water molecule is 1/2 (Petrache et al., 1997), even though lipid headgroup and water are intimately mixed. Volumetric parameters from simulations have been obtained from fits to density histograms (Eq. (4)), and thicknesess from Eq. (6). Simulated thicknesses and overall lipid volumes are within 1.5% of experimental results, as shown in Table 1. For DMPC, we obtain $V_L = 1085$ Å^3 compared to 1101 Å^3 from experiment (Petrache et al., 1998b). For DPPC, we obtain $V_L = 1223$ Å^3 versus 1232 Å (Nagle et al., 1996). Consistent with previous simulation results, component volumes, i.e. headgroup and acyl chains show somewhat larger deviations from experiment (Petrache et al., 1997; Armen et al., 1998). One reason is that component volumes are not determined directly by experiment, and therefore have a larger uncertainty. For example, headgroup volumes between 319 and 340 Å^3 have been suggested (Tristram-Nagle et al., 2002). For the experimental columns in Table 1 we consider a value of 319 Å^3 as a temperature and lipid-independent

Table 1
Bilayer structural parameters

	DMPC[a]	DMPC^{exp}	DPPC[b]	DPPC^{exp}
A	59.7	59.6	62.9	64.0
V_L	1085	1101	1223	1232
V_W	29.9	30.0	30.3	30.3
V_2	27.7	28.1	28.2	28.7
V_3	51.8	53.8	54.4	54.7
V_H	316.9	319	323.3	319
V_C	768.0	782	899.4	913
D_B	36.3	36.9	38.9	38.5
D_C	12.9	13.1	14.3	14.3
D_H	5.3	5.4	5.1	5.0

[a] DMPC simulation at 30 °C compared with experimental data (DMPC^{exp}) from Petrache et al. (1998b).

[b] DPPC simulation at 50 °C vs. experimental results (DPPC^{exp}) from Nagle and Tristram-Nagle (2000). From simulations, volumes are calculated through density histogram fits, then thicknesses (D_B, D_C, D_H) are calculated using Eq. (6) as explained in Section 2. Dimensional units are Å. A denotes the area per lipid (fixed in the simulation); volumes are denoted by V_L (lipid), V_W (water), V_2 (methylene), V_3 (methyl), V_H (headgroup), and V_C (hydrocarbon chains).

reference value as in Nagle and Tristram-Nagle (2000).

The two simulated lipid bilayers differ in their volumetric thicknesses by $\Delta D_C = D_C^{DPPC} - D_C^{DMPC} = 1.4\,Å$, and $\Delta D_B/2 = 1.3\,Å$. As mentioned in Section 1, ΔD_C is of particular interest for determination of the area per lipid from the head–head spacing shift ΔD_{HH}. What is the relationship between D_C and D_{HH} if Fourier truncation is taken into account? For this, we shift our focus from the physical picture to the mathematical abstraction implicit in the treatment of $F(q)$ and $\rho^*(z)$. For a range of D-spacings, we have sampled the simulated $F(q)$ transforms at points $q_h = 2\pi h/D$, for $h = 1, 2, 3, 4$. We then reconstructed $\rho^*(z)$ distributions using Eq. (1). Due to Fourier truncation, the resulting profiles plotted in Fig. 3A are smoother than the original $\rho^*(z)$. Importantly, the headgroup peaks shift. D_{HH} values from these reconstructed (smoothed) profiles are shown in Fig. 3B for a broad range of D-spacings. Interpreting the shift in D_{HH} relies on the choice of this range, for which we highlight three possibilities in Fig. 3B. At the first level, one can consider a broad D-spacing range to study the overall mathematical behavior of D_{HH}. Second, however, only a finite D-spacing range is available experimentally for each lipid. Finally, this range is further reduced for samples with four orders of diffraction. In this narrow, but here most relevant D-spacing range, Fourier truncation makes D_{HH} appear as increasing with D, a clear artifact of the reconstruction. Without corrections, one could measure the wrong expansion coefficient upon dehydration as pointed out by Sun et al. (1996a) and Tristram-Nagle et al. (1998) unless calculated at the same resolution, D/h_{max}, as in Rawicz et al. (2000). Note that while the D-spacings for DMPC and DPPC where four orders are available

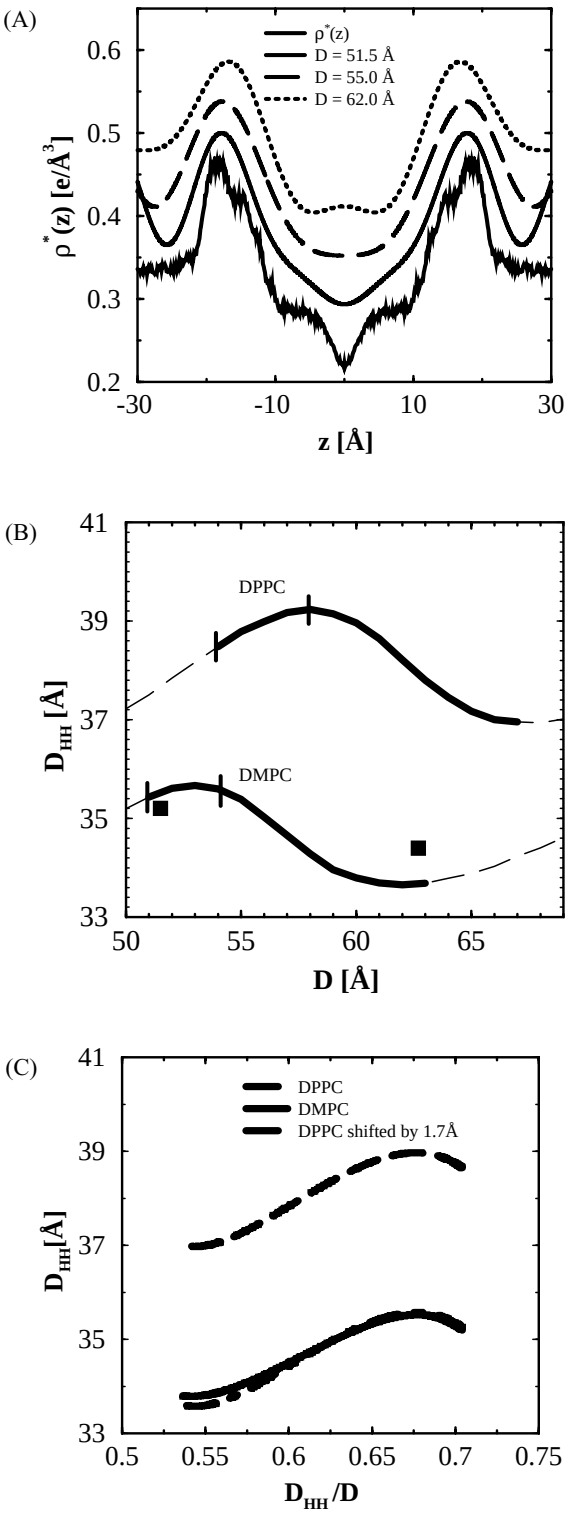

Fig. 3. (A) Effect of Fourier sampling (4 orders) on the shape of DMPC electron density profile. (B) D_{HH} vs. D from simulated reconstruction of $\rho^*(z)$ using 4 orders. Solid lines indicate the range of experimentally available D-spacings, dashed lines cover a wider range available from the simulation. Vertical lines delimit the range of D-spacings for which four orders are measured experimentally. Solid symbols are experimental data points from Petrache et al. (1998b). (C) Data from part (B) recast as D_{HH} vs. D_{HH}/D that shows the constant shift $\Delta D_{HH} = 1.7\,Å$ between DPPC and DMPC.

do not overlap, in average we find a $\Delta D_{HH}/2$ between DMPC and DPPC of about 1.7 Å compared to the ΔD_C value of 1.4 Å (Table 1). Proper comparison of Fourier truncation effects for the two lipids is done as a function of D_{HH}/D as suggested by Sun et al. (1996a). This is shown in Fig. 3C. The two curves are practically the same, apart from a constant shift of 2×1.7 Å over the entire D-spacing range. Applying the bootstrap method with $\Delta D_C \approx \Delta D_{HH}/2 = 1.7$ Å between DMPC and DPPC, it gives hydrocarbon thicknesses within 0.2–0.3 Å, an acceptable 1–2% deviation.

In some cases, experimental techniques provide $F(q)$ over a continuous range of q-values (Pabst et al., 2000; Lyatskaya et al., 2001), but are similarly truncated due to limits of resolution (q_{max}). In order to investigate this, we have truncated $F(q)$ at a range of values, q_{max}, followed by a reverse Fourier transformation. Fig. 4 plots D_{HH} as a function of q_{max}. The data show that the range of D_{HH} decreases as q_{max} increases, with $34.2\,\text{Å} \leq D_{HH}^{DMPC} \leq 35.0\,\text{Å}$ and $37.5\,\text{Å} \leq D_{HH}^{DPPC} \leq 38.4\,\text{Å}$ given q_{max} is taken in the range of the fourth order peak. $\Delta D_{HH}/2$ is, in average 1.7 Å, with values between 1.4 and 2.1 Å if taken at equal values of q_{max}.

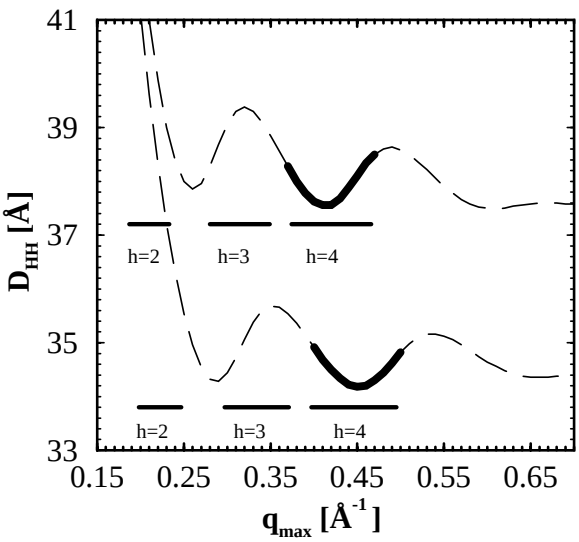

Fig. 4. Variation of D_{HH} with the q_{max} cutoff from the inverse Fourier transform of the simulated $F(q)$. The horizontal lines show the range of experimentally measured form factors, and provide a natural reference for the q_{max} values considered. Solid lines highlight the D_{HH} variation within the $h_{max} = 4$ range.

3.2. Absolute scale determination

Noting the discrepancy between the simulated and experimental $F(q)$ for DMPC in Fig. 2, we now test the method for setting the scale used in Petrache et al. (1998b). The experimental scale was determined from a headgroup integral defined relative to the water level,

$$\text{AH} = \int_{D_C}^{D/2} [\rho^*(z) - \rho_W^*]\,dz \approx n_H^* - \rho_W^* V_H. \qquad (9)$$

The analytical expression on the right hand side is obtained with the assumption that there is only water, and no hydrocarbon mixed with the headgroups. With $n_H^* = 164e$, $V_H = 319\,\text{Å}^3$, and $\rho_W^* = 0.333\,\text{electrons/Å}^3$, the value of AH is then expected to be $57.7e$ at 30 °C. Thus, in Petrache et al. (1998b), the reconstruction of $\rho^*(z)$ from the form factor ratios using Eq. (1) was iterated until a choice for F_1 yielded $\text{AH} = 57.7e$ for the integral in Eq. (9). We are now in a position to verify this assumption using the simulated profiles. Headgroup integrals from the water baseline, as in the above equation, are given in Table 2 together with the evaluation of the analytical result, $n_H^* - \rho_W^* V_H$. The analytical form gives the expected values, but the integral forms are lower by about 14%. This suggests that using the above integral overestimates the height of the headgroup peak and implicitly the overall amplitude of $F(q)$. The scale used in Petrache et al. (1998b) is possibly overestimated (Huber, 1999; Huber and Beyer, 2000). The assumption that water and hydrocarbon do not mix in the headgroup region, required for application of Eq. (9), was an oversimplification. The problem is solved by a better choice for the baseline, as shown in Fig. 5. The left-hand side of Fig. 5 shows the contribution of water, $\rho_W^*(z)$, and hydrocarbon, $\rho_C^*(z)$, to the total electron density profile. If these two distributions are subtracted from the total $\rho^*(z)$, the remaining is just the headgroup part which integrates to $n_H^* = 164e$. These component profiles, however, are hard to determine from experiments. It is more feasible to consider the associated Gibbs dividing surfaces, located by definition at $z = D_C$ and $z = D_B/2$ (Section 2). The original $\rho_W^*(z)$ and $\rho_C^*(z)$ are now replaced by step functions with plateau values $\rho_W^* = 10e/V_W$ and $\rho_2^* = 8e/V_2$. By construction, if these step functions are subtracted from $\rho^*(z)$ the remaining part (excluding the methyl

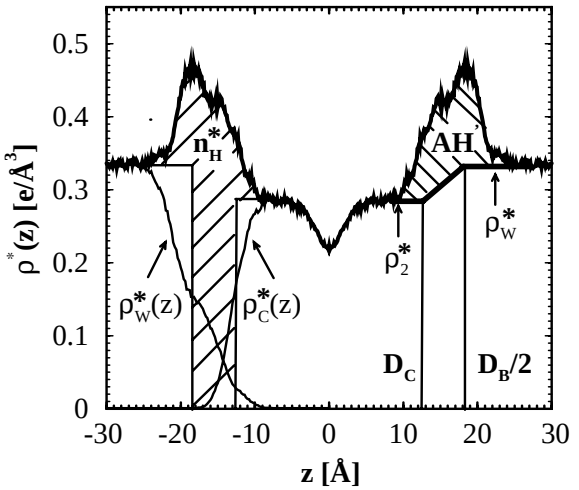

Fig. 5. DMPC electron density profile, $\rho^*(z)$, demonstrating the new integral, AH′, (Eq. (10)) for setting $\rho^*(z)$ on an absolute scale. On the left, the hashed area is approximately equal to n_H^* when multiplied by A. On the right, AH′ results from subtraction of the trapezoidal area below the baseline, defined by the electron densities ρ_2^* and ρ_W^* and the distance $D_H = D_B/2 - D_C$.

region at the bilayer center) integrates to $\approx n_H^*$, as we have verified for both DMPC and DPPC simulations (obtained 163.2e and 161.7e, respectively). The new choice for the headgroup peak baseline is shown on the right side of Fig. 5. The new headgroup integral is

$$\mathrm{AH}' = n_H^* - \frac{\rho_2^* + \rho_W^*}{2} V_H, \tag{10}$$

where the negative term on the right-hand side represents the trapezoidal contribution under the tilted baseline. While still a simplification, this integral has the advantage of incorporating knowledge of ρ_2^* in addition to ρ_W^*. Results are given in Table 2 and show a much better agreement (1–4%) between the direct and analytical AH′, compared to 14% for AH. To include the methyl density as well, one could work with the average hydrocarbon density $\rho_C^* = A\int \rho_C^*(z)\,dz/AD_C = n_C^*/V_C$, where n_C^* represents the number of electrons in the hydrocarbon chains (e.g. 210e for DMPC). In this case, the lower bounds of the hashed area on the right-hand side of Fig. 5 are extended to the center of the bilayer. Results using ρ_C^* (not shown) are comparable to those using ρ_2^*.

4. Discussion

Guided by molecular dynamics simulations of DMPC and DPPC, we have taken a critical look at the Fourier reconstruction method used to obtain structural parameters from X-ray. We have addressed two main aspects. First, we have estimated the effect of Fourier truncation on the headgroup peak location, and the uncertainty in measuring ΔD_C using the headgroups peaks. We have used smoothed (4-order) electron density profiles corresponding to the typical resolution achievable by experiments. Between DMPC at 30 °C and DPPC at 50 °C we find $\Delta D_{HH}/2 \approx 1.7$ Å compared to the hydrocarbon thickness difference $\Delta D_C = 1.4$ Å. Given the many possible sources for discrepancy (including choice of bin size, volumetric decomposition, etc.) these values are in close proximity. Applying the bootstrap method to simulations, it predicts hydrocarbon thicknesses within 1–2%, an acceptable uncertainty level for structural parameters. While D_{HH} values are strongly affected by Fourier truncation, these effects cancel out in the calculation of ΔD_{HH} between two lipids, if comparison is done at the same value of D_{HH}/D, as suggested by Sun et al. (1996a,b), and shown here in Fig. 3. (We also noted that if comparison is made at the same water spacing, $\Delta D_{HH}/2$ is brought closer to ΔD_C, within 0.1 Å, for small D. However, in a real experimental situation this approach is circular, as the area per lipid is needed for calculation of D_W.)

Table 2
Headgroup peak integrals (number of electrons per lipid)

	AH			AH′		
	Integral	Analytical	Dev (%)	Integral	Analytical	Dev (%)
DMPC	49.5	57.8	14.4	64.4	65.2	1.2
DPPC	50.1	58.3	14.0	62.6	64.9	3.5

Second, taking advantage of internal consistency of all-atom simulations we have proposed an improved, yet convenient method to set the experimentally reconstructed profile on an absolute scale using the headgroup peak integral. The difference with the previous method (Petrache et al., 1998b) is in the construction of the baseline, as shown in Fig. 5. In addition to ρ^*_W, the new construction also needs ρ^*_C, D_C and D_B, which are calculated from volumetric data, before the scale is determined. We note that the resulting jagged baseline is a simplified version of the smooth (sinusoidal) "bridging function" employed by Wiener et al. (1989) in their hybrid Gaussian model. In most practical situations, one could eventually use a straight, tilted line to replace the baseline in Fig. 5, or consider variations as discussed in detail by Nagle and Wiener (1989).

Given the form factor ratios F_h/F_1 for a particular sample, the scaling procedure should now consist of finding the F_1 value for which Eq. (10) is satisfied. The previous method converges at large values of F_1 to make up for contributions missed by the flat baseline; this gives a 14% deviation as shown in Table 2. The new method can bring F_1 within 1–4% of the true value. In principle, given many orders of diffraction one can find the absolute scale by normalizing the scattering intensity using Parceval's theorem (Worthington, 1969; Blaurock et al., 1971). For fluid bilayers, however, the uncertainty could be large because higher order peaks are undetectable due to bilayer fluctuations (discussed below) (Nagle and Tristram-Nagle, 2000). Another way to fix the scale is by using halogenated molecular labels as proposed by Franks et al. (1978), if feasable.

Since the experimental electron density profiles are derived quantities, we have compared simulated continuous transforms $F(q)$ with the experimentally measured form factors F_h (Fig. 2). For the two lipids considered, we have found an overall agreement between the simulated and the experimental data, especially in the first and second lobes of $F(q)$. A slight shift in the position of the first lobe is seen due to small differences in bilayer thicknesses D_B between simulation and experiment (Table 1). Significant deviations are seen for the 4th orders. In order to examine the effect of F_4 uncertainty, Fig. 6 compares simulated and experimental DMPC profiles using 4 orders for $D = 51.5$ Å (diamond symbols in Fig. 2A). The two sets of form factors differ only by the value of

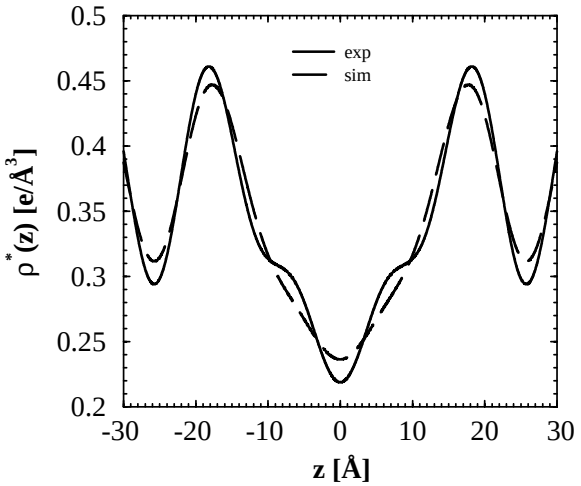

Fig. 6. Comparison of experimental and simulated 4-order DMPC profiles for $D = 51.5$ Å. Form factors differ by the value of F_4 (0.9 electrons/Å^2 vs. 0.5 electrons/Å^2; compare diamond symbols with $F(q)$ in Fig. 2A). With increasing F_4, emergence of features in the methylene region accompany overall changes in D_{HH} as well as in the magnitude of the headgroup and methyl regions.

F_4 (the scale was chosen from the simulated $F(q)$ for both). As expected, the effect is propagated throughout the entire profile, with significant changes in the shape of the methylene region as well as in D_{HH}. A change of $\approx$1 Å in D_{HH} is seen, larger than the effect of Fourier truncation in the 4-order range.

From this perspective, it is also interesting to look at the difference $D_{h1} = (D_{HH}/2) - D_C$, which has been experimentally estimated in the range of 4.1–4.9 Å (Petrache et al., 1998b; Nagle and Tristram-Nagle, 2000), and 4.1–5.5 Å (Balgavý et al., 2001). From our simulations we find $D_{h1} = 4.0$–5.0 Å for DMPC and $D_{h1} = 4.2$–5.3 Å for DPPC, depending on the chosen D-spacing. The larger values are given by the small D-spacings. If we focus on the D-spacings for which there are four orders available, D_{h1} range shrinks considerably, to 4.8–4.9 Å for DMPC and 5.0–5.3 Å for DPPC. A value of 4.9 Å was used by Nagle and Tristram-Nagle (2000). One difference between our simulation analysis and experiment is that that for the real system, D_C increases by 0.5–0.8 Å with reduction of D (due to osmotic stress), while in our analysis it is fixed. This correlates with the D_{HH} difference seen in Fig. 6, where simulation is compared to a reconstructed density profile obtained from a DMPC

sample under 27 atm of osmotic pressure. Because the bilayer is laterally compressible, osmotic stress reduces cross-sectional area and increases the hydrocarbon thickness. At 27 atm, DMPC cross-sectional area decreases by about 2.8%.

Despite inherent limitations, the simulations have provided an internally consistent evaluation of Fourier truncation errors. As shown in Fig. 3, one sees an artifactual change of D_{HH} with D even though the membrane thickness is fixed. The magnitude of these artifacts is significant, on the order of 1–2 Å for the full D-spacing range. This apparent thickness variation is larger than what is allowed by bilayer compressibility. As shown by the corrected experimental data points in Fig. 3B, for DMPC D_{HH} is estimated to decrease by only 0.8 Å from $D = 51.5$ to 62.7 Å, less than the Fourier variation. Furthermore, for small D-spacings corresponding to the 4-order regime, Fourier truncation makes D_{HH} increase with D, clearly an artifact as previously discussed by Tristram-Nagle et al. (1998). These observations highlight the fact that accurate determination of structural parameters from experiment needs consistent treatment of density profiles, by either comparing profiles at the same resolution (McIntosh and Simon, 1986a; Rawicz et al., 2000) and/or by considering corrections to the measured D_{HH} values (Nagle and Tristram-Nagle, 2000).

There is an additional complication when comparing simulated and experimental profiles, namely fluctuations. A critical aspect in determining the true shape of the electron density distribution is that the broad spectrum of molecular fluctuations alters the appearance of $\rho^*(z)$. While main features such as the electron rich headgroup peaks and the electron depleted bilayer center are less dependent on fluctuations, more detailed features such as peak asymmetries and methylene shoulders can exist depending on the extent of in-plane positional correlations. What is measured by X-ray: a local profile (of 100 Å or less), or a global profile (1000 Å or more)? From simulations, size-dependent profiles are obtained (Hofsäß et al., 2003), unless one deconvolves global shape fluctuations. Based on the wide-angle scattering, it is reasonable to assume that in-plane correlations are on the order of 100 Å or less in the fluid phase. For the gel phase, interchain correlations as high as 2900 Å have been measured (Sun et al., 1994), while in the ripple phase, a repeat distance of 120 Å is found (Wack and Webb, 1989; Sun et al., 1996a). This sets an upper limit for the fluid phase in-plane correlations.

With a reduced number of diffraction peaks, the local versus global distinction becomes difficult to define. As expected and shown in this work, Fourier truncation always leads to smoother profiles, and this limits our ability to determine whether electron density profiles for the fluid state are detail-rich or not. Note, for example, that the reconstructed headgroup peaks in Figs. 3 and 6 do not contain the small headgroup shoulder approximately 15–17 Å from the bilayer center seen in Fig. 1. This feature, due to the electron rich carbonyl and glycerol groups, is seen experimentally in the gel-phase (Tristram-Nagle et al., 2002), where 10 orders of diffraction can be measured. Are such features in fact smoothed out by the larger degree of fluctuation in the fluid phase, or do the reconstructed profiles simply miss these details from lack of higher order information? Combining insight from both all-atom simulations and experiment is a fruitful approach to answering such questions.

Acknowledgements

We thank Dr. John F. Nagle for valuable discussions and comments on the manuscript, and Dr. Thomas Huber for discussions of continuous transforms and of his simulation results. J.N.S. thanks the Whitaker Foundation for Biomedical Engineering for graduate fellowship support.

Appendix A

The four component volumes, V_3, V_2, V_H, and V_W are chosen as the values that make the total probability $p_T(z)$ equal to 1 for all z values, i.e. the volume parameters minimize the following function:

$$\chi^2(V_3, V_2, V_H, V_W) = \sum_z [p_T(z) - 1]^2. \quad (A.1)$$

Minimization proceeds by setting the derivative of χ^2 with respect to each volumetic parameter equal to zero. For example, with respect to V_3, we have

$$\frac{d\chi^2}{dV_3} = 2\sum_z [V_3 n_3(z) + V_2 n_2(z) + V_H n_H(z) + V_W n_W(z) - 1]\, n_3(z) = 0 \quad (A.2)$$

The four minimizing conditions then give the following 4×4 system of linear equations:

$$\begin{aligned}
&V_3 \textstyle\sum_z n_3^2 + V_2 \sum_z n_3 n_2 + V_{\mathrm{H}} \sum_z n_3 n_{\mathrm{H}} \\
&\quad + V_{\mathrm{W}} \textstyle\sum_z n_3 n_{\mathrm{W}} = \sum_z n_3 \\
&V_3 \textstyle\sum_z n_2 n_3 + V_2 \sum_z n_2^2 + V_{\mathrm{H}} \sum_z n_2 n_{\mathrm{H}} \\
&\quad + V_{\mathrm{W}} \textstyle\sum_z n_2 n_{\mathrm{W}} = \sum_z n_2 \\
&V_3 \textstyle\sum_z n_{\mathrm{H}} n_3 + V_2 \sum_z n_{\mathrm{H}} n_2 + V_{\mathrm{H}} \sum_z n_{\mathrm{H}}^2 \\
&\quad + V_{\mathrm{W}} \textstyle\sum_z n_{\mathrm{H}} n_{\mathrm{W}} = \sum_z n_{\mathrm{H}} \\
&V_3 \textstyle\sum_z n_{\mathrm{W}} n_3 + V_2 \sum_z n_{\mathrm{W}} n_2 + V_{\mathrm{H}} \sum_z n_{\mathrm{W}} n_{\mathrm{H}} \\
&\quad + V_{\mathrm{W}} \textstyle\sum_z n_{\mathrm{W}}^2 = \sum_z n_{\mathrm{W}}
\end{aligned} \tag{A.3}$$

where the summation argument (z) has been suppressed for simplicity. This system can be set in a matrix form and solved for V_3, V_2, V_{H}, and V_{W} by conventional numerical recipies (e.g. GAUSSJ subroutine from Press et al., 1988). Analysis scripts (CHARMM and Fortran) can be obtained by request or found at http://lpsb.nichd.nih.gov/.

References

Armen, R.S., Uitto, O.D., Feller, S.E., 1998. Phospholipid component volumes: determination and application to bilayer structure calculations. Biophys. J. 75, 734–744.

Balgavý, P., Dubničková, M., Kučerka, N., Kiselev, M.A., Yaradaikin, S.P., Uhríková, D., 2001. Bilayer thickness and lipid interface area in unilamellar extruded 1,2-diacylphosphatidylcholine liposomes: a small-angle neutron scattering study. Biochim. Biophys. Acta 1512, 40–52.

Berger, O., Edholm, O., Jähnig, F., 1997. Molecular dynamics simulations of a fluid bilayer of dipalmitoylphosphatidylcholine at full hydration, constant pressure, and constant temperature. Biophys. J. 72, 2002–2013.

Blaurock, A.E., 1971. Structure of the nerve myelin membrane: proof of the low-resolution profile. J. Mol. Biol. 56, 35–52.

Bloom, M., Evans, E., Mouritsen, O.G., 1991. Physical-properties of the fluid lipid-bilayer component of cell-membranes—a perspective. Q. Rev. Biophys. 24, 293–397.

Bloom, M., Linseisen, F., Lloyd-Smith, J., Crawford, M., 1999. Magnetic resonance and brain function: approaches from physics. In: Maraviglia, B. (Ed.), Proceedings of the June 23–July 3 1998 Enrico Fermi International School of Physics, Course CXXXIX, Varenna, Italy. IOS Press, Amsterdam, 1999, pp. 527–553.

Botelho, A.V., Gibson, N.J., Thurmond, R.L., Wang, Y., Brown, M.F., 2002. Conformational energetics of rhodopsin modulated by non-lamellar-forming lipids. Biochemistry 41, 6354–6368.

Brooks, B.R., Bruccoleri, R.E., Olafson, B.D., States, D., Swaminathan, S., Karplus, M.J., 1983. CHARMM—a program for macromolecular energy, minimization, and dynamics calculations. J. Comput. Chem. 4, 187–217.

Brown, M.F., 1994. Modulation of rhodopsin function by properties of the membrane bilayer. Chem. Phys. Lipids 73, 159–180.

Chiu, S.-W., Clark, M., Balaji, V., Subramanian, S., Scott, H.L., Jakobsson, E., 1995. Incorporation of surface tension into molecular dynamics simulation of an interface: A fluid phase lipid bilayer membrane. Biophys. J. 69, 1230–1245.

Elliott, J.R., Needham, D., Dilger, J.P., Haydon, D.A., 1983. The effects of bilayer thickness and tension on gramicidin single-channel lifetime. Biochim. Biophys. Acta 735, 95–103.

Franks, N.P., Arunachalam, T., Caspi, E., 1978. A direct method for determination of membrane electron density profile on an absolute scale. Nature 276, 530–532.

Feller, S.E., Pastor, R.W., 1999. Constant surface tension simulations of lipid bilayers: the sensitivity of surface areas and compressibilities. J. Chem. Phys. 111, 1281–1287.

Feller, S.E., Venable, R.M., Pastor, R.W., 1997. Computer simulation of a DPPC phospholipid bilayer: structural changes as a function of molecular surface area. Langmuir 13, 6555–6561.

Greathouse, D.V., Hinton, J.F., Kim, K.S., Koeppe II, R.E., 1994. Gramicidin-A short-chain phospholipid dispersions–chain-length dependence of gramicidin conformation and lipid organization. Biochemistry 33, 4292–4299.

Gruner, S.M., 1989. Stability of lyotropic phases with curved interfaces. J. Phys. Chem. 22, 7562–7570.

Hardy, B.J., Pastor, R.W., 1994. Conformational sampling of hydrocarbon and lipid chains in an orienting potential. J. Comput. Chem. 15, 208–226.

Harroun, T.A., Heller, W.T., Weiss, T.M., Yang, L., Huang, H.W., 1999. Experimental evidence for hydrophobic matching and membrane-mediated interactions in lipid bilayers. Biophys. J. 76, 845–937.

Hofsäß, C., Lindahl, E., Edholm, O., 2003. Molecular dynamics simulations of phopholipid bilayers with cholesterol. Biophys. J. 84, 2192–2206.

Huang, H.W., 1986. Deformation free-energy of bilayer-membrane and its effect on gramicidin channel lifetime. Biophys. J. 50, 1061–1070.

Huber, T., 1999. Ph.D. Thesis. Ludwig Maximilians University, Munich.

Huber, T., Beyer, K., 2000. Multiscale properties of the aqueous boundary of biological membranes from simulation. Biophys. J. 78, 1069.

Huber, T., Rajamoorthi, K., Kurze, V.F., Beyer, K., Brown, M.F., 2002. Structure of docosahexaenoic acid-containing phospholipid bilayers as studied by ^{2}H NMR and molecular dynamics simulations. J. Am. Chem. Soc. 124, 298–309.

Israelachvili, J.N., 1992. Intermolecular and Surface Forces. Academic Press, London.

Katsaras, J., 1995. Structure of the subgel $L_{C'}$ and gel $L_{\beta'}$ phases of oriented dipalmitoylphosphatidylcholine multibilayers. J. Phys. Chem. 99, 4141–4147.

Killian, J.A., Heijne, G.V., 2000. How proteins adapt to a membrane–water interface. Trends Biochem. Sci. 25, 429–434.

Leikin, S., Parsegian, V.A., Rau, D.C., Rand, R.P., 1993. Hydration forces. Annu. Rev. Phys. Chem. 44, 369–395.

Lesslauer, W., Cain, J.E., Blasie, J.K., 1972. X-ray diffraction studies of lecithin biomolecular leaflets with incorporated fluorescent probes. Proc. Natl. Acad. Sci. 69, 1499–1503.

Lyatskaya, Y., Liu, Y.F., Tristram-Nagle, S., Katsaras, J., Nagle, J.F., 2001. Method for obtaining structure and interactions from oriented lipid bilayers. Phys. Rev. E 63, 011907.

Marsh, D., 1989. Water adsorption isotherms and hydration forces for lysolipids and diacyl phospholipids. Biophys. J. 55, 1093–1100.

Mashl, R.J., Scott, H.L., Subramaniam, S., Jakobsson, E., 2001. Molecular simulation of dioleoylphophatidylcholine lipid bilayers at differing levels of hydration. Biophys. J. 81, 3005–3015.

McIntosh, T.J., Simon, S.A., 1986a. Hydration force and bilayer deformation—a reevaluation. Biochemistry 25, 4058–4066.

McIntosh, T.J., Simon, S.A., 1986b. Area per molecule and distribution of water in fully hydrated dilauroylphosphatidylethanolamine. Biochemistry 25, 4948–4952.

McIntosh, T.J., Simon, S.A., 1993. Contributions of hydration and steric (entropic) pressures to the interactions between phophatidylcholine bilayers: experiments with the subgel phase. Biochemistry 32, 8374–8384.

Nagle, J.F., Wiener, M.C., 1989. Relations for lipid bilayers—connection of electron-density profiles to other structural quantities. Biophys. J. 55, 309–313.

Nagle, J.F., Tristram-Nagle, S., 2000. Structure of lipid bilayers. Biochim. Biophys. Acta 1469, 159–195.

Nagle, J.F., Zhang, R., Tristram-Nagle, S., Sun, W.-J., Petrache, H.I., Suter, R.M., 1996. X-ray structure determination of fully hydrated L_α phase dipalmitoylphosphatidylcholine bilayers. Biophys. J. 70, 1419–1431.

Pabst, G., Rappolt, M., Amenitsch, H., Laggner, P., 2000. Structural information from multilamellar liposomes at full hydration: full q-range fitting with high quality X-ray data. Phys. Rev. E 62, 4000–4009.

Petrache, H.I., Feller, S.E., Nagle, J.F., 1997. Determination of component volumes of lipid bilayers from simulations. Biophys. J. 72, 2237–2242.

Petrache, H.I., Gouliev, N., Tristram-Nagle, S., Suter, R.M., Nagle, J.F., 1998a. Interbilayer interactions from high-resolution X-ray scattering. Phys. Rev. E 57, 7014–7024.

Petrache, H.I., Tristram-Nagle, S., Nagle, J.F., 1998b. Fluid phase structure of EPC and DMPC bilayers. Chem. Phys. Lipids 95, 83–94.

Petrache, H.I., Grossfield, A., MacKenzie, K.R., Engelman, D.M., Woolf, T.B., 2000. Modulation of glycophorin A transmembrane helix interactions by lipid bilayers: molecular dynamics calculations. J. Mol. Biol. 302, 727–746.

Petrache, H.I., Zuckerman, D.M., Sachs, J.N., Killian, J.A., Koeppe, R.E., Woolf, T.B., 2002. Hydrophobic matching mechanism investigated by molecular dynamics simulations. Langmuir 18, 1340–1351.

Press, W.H., Flannery, B.P., Teukolsky, S.A., Vetterling, W.T., 1988. Numerical Recipies. The Art of Scientific Computing. Cambridge University Press, New York.

Rand, R.P., Parsegian, V.A., 1989. Hydration forces between phospholipid-bilayers. Biochim. Biophys. Acta 988, 351–376.

Rawicz, W., Olbrich, K.C., McIntosh, T.J., Needham, D., Evans, E., 2000. Effect of chain length and unsaturation on elasticity of lipid bilayers. Biophys. J. 79, 328–339.

Schalke, M., Losche, M., 2000. Structural models of lipid surface monolayers from X-ray and neutron reflectivity measurements. Adv. Coll. Int. Sci. 88, 243–274.

Small, D.M., 1996. The Physical Chemistry of Lipids, Handbook of Lipid Research, vol. 4. Plenum Press, New York.

Smondyrev, A.M., Berkowitz, M.L., 1999. Molecular dynamics study of Sn-1 and Sn-2 chain conformations in DPPC membranes. J. Chem. Phys 110, 3981–3985.

Sun, W.J., Suter, R.M., Knewtson, M.A., Worthington, C.R., Tristram-Nagle, S., Zhang, R., Nagle, J.F., 1994. Order and disorder in fully hydrated unoriented bilayers of gel phase DPPC. Phys. Rev. E 49, 4665–4676.

Sun, W.J., Tristram-Nagle, S., Suter, R.M., Nagle, J.F., 1996a. Structure of gel phase saturated lecithin bilayers: temperature and chain length dependence. Biophys. J. 71, 885–891.

Sun, W.J., Tristram-Nagle, S., Suter, R.M., Nagle, J.F., 1996b. Structure of the ripple phase in lecithin bilayers. Proc. Natl. Acad. Sci. 93, 7008–7012.

Tieleman, D.P., Marrink, S.J., Berendsen, H.J.C., 1997. A computer perspective of membranes: molecular dynamics studies of lipid bilayer systems. Biochim. Biophys. Acta 1331, 235–270.

Tobias, D.J., Tu, K.C., Klein, M.L., 1997. Atomic-scale molecular dynamics simulations of lipid membranes. Current Opin. Colloid Interf. Sci. 2, 15–26.

Tristram-Nagle, S., Suter, R.M., Sun, W.-J., Nagle, J.F., 1994. Kinetics of subgel formation in DPPC—X-ray-diffraction proves nucleation-growth hypothesis. Biochim. Biophys. Acta 1991, 14–20.

Tristram-Nagle, S., Petrache, H.I., Nagle, J.F., 1998. Structure and interactions of fully hydrated dioleoylphosphatidylcholine bilayers. Biophys. J. 75, 917–925.

Tristram-Nagle, S., Liu, Y.F., Legleiter, J., Nagle, J.F., 2002. Structure of gel phase DMPC determined by X-ray diffraction. Biophys. J. 83, 3324–3335.

Wack, D.C., Webb, W.W., 1989. Synchrotron X-ray study of the modulated lamellar phase in the lecithin–water system. Phys. Rev. A 40, 2712–2730.

Wiener, M.C., White, S.H., 1992. Structure of a fluid dioleoylphosphatidylcholine bilayer determined by joint refinement of X-ray and neutron-diffraction data. 3. Complete structure. Biophys. J. 61, 434–447.

Wiener, M.C., Suter, R.M., Nagle, J.F., 1989. Structure of the fully hydrated gel phase of DPPC. Biophys. J. 55, 315–325.

Worthington, C.R., 1969. Interpretation of low-angle X-ray data from planar and concentric multilayered structures—use of one-dimensional electron density strip models. Biophys. J. 9, 222–234.

Zimmerberg, J., Chernomordik, L.V., 1999. Membrane fusion. Adv. Drug Deliv. Rev. 38, 197–205.